Eurographics/ ACM SIGGRAPH Symposium on Computer Animation (2014)
Vladlen Koltun and Eftychios Sifakis (Editors)

Stable Orthotropic Materials

Yijing Li and Jernej Barbič

University of Southern California, United States

Abstract

Isotropic Finite Element Method (FEM) deformable object simulations are widely used in computer graphics. Several applications (wood, plants, muscles) require modeling the directional dependence of the material elastic properties in three orthogonal directions. We investigate orthotropic materials, a special class of anisotropic materials where the shear stresses are decoupled from normal stresses. Orthotropic materials generalize transversely isotropic materials, by exhibiting different stiffnesses in three orthogonal directions. Orthotropic materials are, however, parameterized by nine values that are difficult to tune in practice, as poorly adjusted settings easily lead to simulation instabilities. We present a user-friendly approach to setting these parameters that is guaranteed to be stable. Our approach is intuitive as it extends the familiar intuition known from isotropic materials. We demonstrate our technique by augmenting linear corotational FEM implementations with orthotropic materials.

Categories and Subject Descriptors (according to ACM CCS): I.3.6 [Computer Graphics]: Methodology and Techniques—Interaction Techniques, I.6.8 [Simulation and Modeling]: Types of Simulation—Animation

1. Introduction

Simulation of three-dimensional solid deformable models is important in many applications in computer graphics, robotics, special effects and virtual reality. Most applications in these fields have been limited to isotropic materials, i.e., materials that are equally elastic in all directions. Many real materials are, however, stiffer in some directions than others. The space of such anisotropic materials is vast and not easy to navigate, tune or control. In this paper, we study orthotropic materials. Orthotropic materials exhibit different stiffness in three orthogonal directions; formally, they possess three orthogonal planes of rotational symmetry. They form an intuitive subset of all anisotropic materials, as they generalize the familiar isotropic, and transversely isotropic, materials to materials with three different stiffness values in some three orthogonal directions. Although simpler than fully general anisotropic materials, orthotropic materials still require tuning nine independent parameter values. In practice, this task is difficult due to the large number of parameters and because many of the settings lead to unstable simulations in a non-obvious way. In this paper, we study orthotropic materials from the point of view of practical simulation in computer graphics and related fields. We demonstrate how to intuitively and stably tune orthotropic material parameters, by parameterizing the six Poisson's ratios using a stable one-dimensional parameter family, similar to the intuition from isotropic simulation. This makes it possible to easily augment existing simulation solvers with stable and intuitive anisotropic effects. We support large deformations using corotational Finite Element Method simulation.

2. Related Work

Anisotropic materials are discussed in many references, see, e.g. [Bow11]. Transversely isotropic hyperelastic materials were presented by Bonet and Burton [BB98]. Picinbono et al. [PDA01] proposed a non-linear FEM model to simulate soft tissues with large deformations and transversely isotropic behavior. Thije et al. [TTAH07] addressed the instabilities that occur under strong anisotropy, and provided a simple updated Lagrangian FEM scheme to handle the problem. Picinbono et al. [PLDA00] described a surgery simulator that can model linear transversely isotropic materials at haptic rates and also presented a nonlinear transversely isotropic model for medical simulation [PDA03]. Sermesant et al. [SCD*01, SDA06] and Talbot et al. [TMD*13] adopted a transversely isotropic material in constructing an electromechanical model of the heart. Allard et al. [AMC*09] used a 2D anisotropic material to simulate thin soft tissue tearing,

Comas et al. [CTA*08] implemented a transversely isotropic visco-hyperelastic model on the GPU, and Teran [TSB*05] and Sifakis [SNF05, Sif07] simulated human muscles with a transversely isotropic, quasi-incompressible model. Irving et al. [ITF04] proposed a robust, large-deformation invertible simulation method and demonstrated it with transversely isotropic models. Previous anisotropic applications in computer graphics focused on transversely isotropic materials where two directions have equal stiffness, leading to five tunable parameters. We generalize materials to orthotropic materials with three distinct stiffnesses in three orthogonal directions, and present an intuitive approach to tune the resulting nine parameters. To the best of our knowledge, we are first work in computer graphics to analyze orthotropic materials in substantial detail. Previous papers on orthotropic materials in engineering assumed that the nine orthotropic parameters are given or measured from real materials [VBCW81], whereas we provide an intuitive way for the users to tune them and ensure they are stable. Our work uses corotational linear FEM materials introduced in [MG04]. Construction of the stiffness matrix for linear FEM materials can also be found, for example, in [Sha90].

3. Orthotropic Materials

We now introduce orthotropic materials. Given the deformation gradient F, the Green-Lagrange strain is defined as $\varepsilon^{3\times3} = (F^TF - I)/2$, and the Cauchy stress $\sigma^{3\times3}$ gives the elastic forces per surface area in a unit direction n, as $\sigma^{3\times3}n$ [Sha90]. Note that we can operate with Cauchy stresses here as they are equivalent to other forms of stresses (Piola) due to the small-deformation analysis; we achieve large deformations via co-rotational linear FEM [MG04]. The 6×6 elasticity tensor $\mathscr{S}$ relates strain ε to stress σ via $\varepsilon = \mathscr{S}\sigma$, where we have unrolled the 3×3 symmetric matrices $\varepsilon^{3\times3} = [\varepsilon_{ij}]_{ij}$ and $\sigma^{3\times3} = [\sigma_{ij}]_{ij}$ into 6-vectors, using the 12, 23, 31 ordering of the shear components as in [Sha90]:

$$\varepsilon = [\varepsilon_{11}\ \varepsilon_{22}\ \varepsilon_{33}\ 2\varepsilon_{12}\ 2\varepsilon_{23}\ 2\varepsilon_{31}]^T, \tag{1}$$

$$\sigma = [\sigma_{11}\ \sigma_{22}\ \sigma_{33}\ \sigma_{12}\ \sigma_{23}\ \sigma_{31}]^T. \tag{2}$$

Components $11, 22, 33$ are called normal components, whereas $12, 23, 31$ are referred to as shear components. The inverse elasticity tensor $\mathscr{C} = \mathscr{S}^{-1}$ relates σ to ε, via $\sigma = \mathscr{C}\varepsilon$. The elasticity tensor must be symmetric and therefore it has 21 independent entries for a general anisotropic material,

$$\mathscr{C} = \begin{bmatrix} \mathscr{C}_{11} & \mathscr{C}_{12} & \mathscr{C}_{13} & \mathscr{C}_{14} & \mathscr{C}_{15} & \mathscr{C}_{16} \\ & \mathscr{C}_{22} & \mathscr{C}_{23} & \mathscr{C}_{24} & \mathscr{C}_{25} & \mathscr{C}_{26} \\ & & \mathscr{C}_{33} & \mathscr{C}_{34} & \mathscr{C}_{35} & \mathscr{C}_{36} \\ & & & \mathscr{C}_{44} & \mathscr{C}_{45} & \mathscr{C}_{46} \\ & \textit{Sym.} & & & \mathscr{C}_{55} & \mathscr{C}_{56} \\ & & & & & \mathscr{C}_{66} \end{bmatrix}. \tag{3}$$

Once $\mathscr{C}$ is known, the stiffness matrix for a linear tetrahedral element is computed as $K^e = V^e B^{eT} \mathscr{C}^e B^e$, where V^e is volume of tet e, and B^e is a 6×12 matrix determined by the initial shape of tet e (see [Sha90] or [MG04]).

Unlike isotropic materials that are parameterized by a single Young's modulus and Poisson's ratio, orthotropic materials have three different Young's moduli E_1, E_2, E_3, one for each orthogonal direction, and six Poisson's ratios ν_{ij}, for $i \neq j$, only three of which are independent. Young's modulus E_i gives the stiffness of the material when loaded in orthogonal direction i. Poisson's ratio ν_{ij} gives the contraction in direction j when the extension is applied in direction i. In a general anisotropic material, both the normal and shear components of strain affect both the normal and shear components of stress, i.e., matrix $\mathscr{C}$ is dense. In orthotropic materials, however, the normal and shear components are decoupled: normal stresses only cause normal strains, and shear stresses only cause shear strains. Furthermore, individual shear stresses in the $12, 23, 31$ planes are decoupled from each other: strain ε_{ij} $(i \neq j)$ only depends on stress σ_{ij} via a scalar parameter (shear modulus) μ_{ij}. Under these assumptions, the elasticity tensor has 9 free parameters and takes a block-diagonal form. It is easiest to first state its inverse

$$\mathscr{S}_{ortho} = \begin{bmatrix} \frac{1}{E_1} & -\frac{\nu_{21}}{E_2} & -\frac{\nu_{31}}{E_3} & 0 & 0 & 0 \\ -\frac{\nu_{12}}{E_1} & \frac{1}{E_2} & -\frac{\nu_{32}}{E_3} & 0 & 0 & 0 \\ -\frac{\nu_{13}}{E_1} & -\frac{\nu_{23}}{E_2} & \frac{1}{E_3} & 0 & 0 & 0 \\ 0 & 0 & 0 & \frac{1}{\mu_{12}} & 0 & 0 \\ 0 & 0 & 0 & 0 & \frac{1}{\mu_{23}} & 0 \\ 0 & 0 & 0 & 0 & 0 & \frac{1}{\mu_{31}} \end{bmatrix}. \tag{4}$$

The orthotropic elasticity tensor is then

$$\mathscr{C}_{ortho} = \mathscr{S}_{ortho}^{-1} = \begin{bmatrix} A & 0 \\ 0 & B \end{bmatrix}, \text{ for} \tag{5}$$

$$A = \Upsilon \begin{bmatrix} E_1(1-\nu_{23}\nu_{32}) & E_2(\nu_{12}+\nu_{32}\nu_{13}) & E_3(\nu_{13}+\nu_{12}\nu_{23}) \\ E_1(\nu_{21}+\nu_{31}\nu_{23}) & E_2(1-\nu_{13}\nu_{31}) & E_3(\nu_{23}+\nu_{21}\nu_{13}) \\ E_1(\nu_{31}+\nu_{21}\nu_{32}) & E_2(\nu_{32}+\nu_{12}\nu_{31}) & E_3(1-\nu_{12}\nu_{21}) \end{bmatrix}, \tag{6}$$

$$B = \begin{bmatrix} \mu_{12} & 0 & 0 \\ 0 & \mu_{23} & 0 \\ 0 & 0 & \mu_{31} \end{bmatrix}, \text{ and} \tag{7}$$

$$\Upsilon = \frac{1}{1-\nu_{12}\nu_{21}-\nu_{23}\nu_{32}-\nu_{31}\nu_{13}-2\nu_{21}\nu_{32}\nu_{13}}. \tag{8}$$

Equations 4 and 5 give elasticity tensors with respect to the world coordinate axes. A general orthotropic material, however, assumes the block-diagonal form given in Equations 4 and 5 only in a special orthogonal basis, given by the three principal axes where the stiffnesses are E_1, E_2, E_3. In other bases (including world-coordinate axes), its form looks generic, as in Equation 3. Therefore, to model orthotropic materials whose principal axes are not aligned with the world axes, we need to convert elasticity tensors from one basis to another. For a basis given by a rotation Q, the

elasticity tensor $\mathscr{C}$ transforms as follows:

$$\mathscr{C}_{world} = K\mathscr{C}_{local}K^T, K = \begin{bmatrix} K^{(1)} & 2K^{(2)} \\ K^{(3)} & K^{(4)} \end{bmatrix}, \quad \text{for} \qquad (9)$$

$$K^{(1)}_{i,j} = Q^2_{i,j}\,, \qquad K^{(2)}_{i,j} = Q_{i,j}Q_{i,(j+1)\bmod 3}\,, \qquad (10)$$

$$K^{(3)}_{i,j} = Q_{i,j}Q_{(i+1)\bmod 3,j}\,, \qquad (11)$$

$$K^{(4)}_{i,j} = Q_{i,j}Q_{(i+1)\bmod 3,(j+1)\bmod 3} + \qquad (12)$$

$$+Q_{i,(j+1)\bmod 3}Q_{(i+1)\bmod 3,j}\,. \qquad (13)$$

The rotation matrix Q is an input parameter for constructing the orthotropic material, and can vary spatially on the model (our cylinder and fern examples). It can be made, for example, to correspond to the directional derivatives of a 3D *uvw* texture map.

3.1. Special cases

When two of the three orthogonal directions are equally stiff, one obtains the *transversely isotropic* material. For such a material, there is a plane in which the material is isotropic, but the orthogonal direction is not. There are 5 free parameters, E_p, E_z and ν_p, ν_{pz} and μ_{zp}, and we have $E_1 = E_2 = E_p, E_3 = E_z, \nu_{12} = \nu_{21} = \nu_p, \nu_{13} = \nu_{23} = \nu_{pz}, \nu_{31} = \nu_{32} = \nu_{zp} = \nu_{pz}E_z/E_p, \mu_{12} = E_p/2(1+\nu_p), \mu_{23} = \mu_{31} = \mu_{zp}$. A further simplification is the isotropic material which has just two free parameters E and ν and we have $E_1 = E_2 = E_3 = E$, $\nu_{ij} = \nu$ for all i, j and $\mu_{12} = \mu_{23} = \mu_{31} = E/2(1+\nu)$.

4. Setting the orthotropic parameters

In order to keep the elasticity tensor symmetric, the Poisson's ratios have to satisfy

$$\frac{\nu_{ij}}{E_i} = \frac{\nu_{ji}}{E_j}, \qquad (14)$$

for all $i \neq j$. Therefore, only 3 of the 6 Poisson's ratio are independent. This leaves a total of 9 free parameters in the orthotropic material: $E_1, E_2, E_3, \nu_{12}, \nu_{23}, \nu_{31}, \mu_{12}, \mu_{23}, \mu_{31}$. There are limitations on these 9 parameters. In order for the elastic strain energy of the orthotropic material to be a positive-definite function of ε, the elasticity tensor $\mathscr{C}_{ortho}$ must be positive-definite. Because it is block-diagonal, this condition is equivalent to $\mu_{12} > 0, \mu_{23} > 0, \mu_{31} > 0$ plus positive-definiteness of the upper-left 3×3 block of $\mathscr{C}_{ortho}$. Using the Sylvester's theorem [HJ85], this is equivalent to

$$E_1 > 0, \qquad E_2 > 0, \qquad E_3 > 0, \qquad (15)$$

$$\nu_{12}\nu_{21} < 1, \quad \nu_{23}\nu_{32} < 1, \quad \nu_{31}\nu_{13} < 1, \quad \Upsilon > 0. \qquad (16)$$

These restrictions can be easily derived by examining the upper-left 3×3 block of $\mathscr{S}_{ortho}$ [Lem68].

Unlike the isotropic case where it is well-known that the Poisson's ratio ν has to be on the interval $(-1, 1/2)$, there is no analogous limits on ν_{ij} for orthotropic materials. In practice, it is very tedious to tune these parameters, as suboptimal values easily cause the simulation to explode, or introduce undue stiffness or other poor simulation behavior.

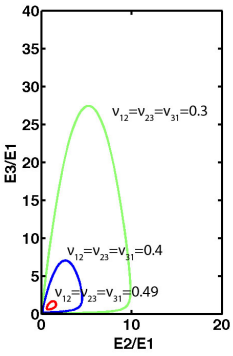

Figure 1: ***Stability of orthotropic materials.*** *The curves show the boundary of the stability region for the naive choice $\nu_{12} = \nu_{23} = \nu_{31}$; the other ν_{ij} are determined via (14).*

We demonstrate the shape of the stability regions in Figure 1, for the naive choice where $\nu_{12}, \nu_{23}, \nu_{31}$ are made equal. The range of Young's modulus ratios which satisfies the positive-definiteness conditions (15) and (16) is limited to the regions shown in the figure. The stability region becomes smaller as ν_{ij} approaches 0.5. Such a simple choice of ν_{ij} greatly limits the range of stable Young's modulus ratios along the three principal axes. Therefore, we propose a scheme to tune the orthotropic materials using the familiar intuition from the isotropic case. Our scheme provably guarantees positive-definiteness of the elasticity tensor. By applying (14) into (16), we obtain

$$\nu^2_{12} < \frac{E_1}{E_2}, \qquad \nu^2_{23} < \frac{E_2}{E_3}, \qquad \nu^2_{31} < \frac{E_3}{E_1}. \qquad (17)$$

Guided by the intuition from isotropic materials, we would like to use one parameter to simplify and control the assignments of all ν_{ij}. Equation 17 imposes upper and lower limits on all the three free ν_{ij} parameters. We control these three parameters using a single Poisson's ratio-like parameter ν as

$$\nu_{12} = \nu\sqrt{\frac{E_1}{E_2}}, \qquad \nu_{23} = \nu\sqrt{\frac{E_2}{E_3}}, \qquad \nu_{31} = \nu\sqrt{\frac{E_3}{E_1}}. \qquad (18)$$

All three restrictions on ν_{ij} from (17) are satisfied by imposing $-1 < \nu < 1$. Using (14) and (18), we can express Υ as

$$\Upsilon = \frac{1}{(1+\nu)^2(1-2\nu)}. \qquad (19)$$

To ensure $\Upsilon > 0$, we need to set $-1 \neq \nu < \frac{1}{2}$. Therefore, to ensure a positive-definite elasticity tensor $\mathscr{C}_{ortho}$, ν must satisfy the condition $-1 < \nu < \frac{1}{2}$. This is the familiar condition known with isotropic materials. Once ν has been selected, we can then use equation (18) to safely determine all ν_{ij}. Figure 2 demonstrates the volume-preservation effect of our orthotropic materials for three values of ν. For transversely isotropic materials, our formula simplifies to

$$\nu_{pz} = \nu_p\sqrt{\frac{E_p}{E_z}}. \qquad (20)$$

In an orthotropic material, the shear moduli μ_{ij} are independent of E and ν. Suboptimal values of shear parame-

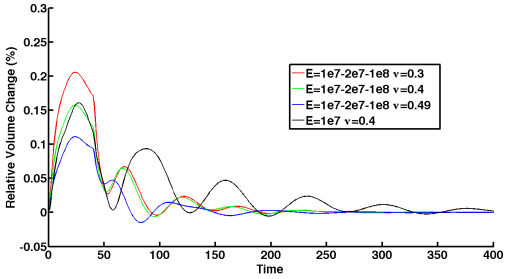

Figure 2: ***Controlling volume preservation with a single parameter ν.*** *Orthotropic dinosaur; stiffnesses are 1E7, 2E7, 1E8. Simulated under three Poisson's ratios $\nu = 0.3, 0.4, 0.49$. Isotropic material ($\nu = 0.4$) is shown black.*

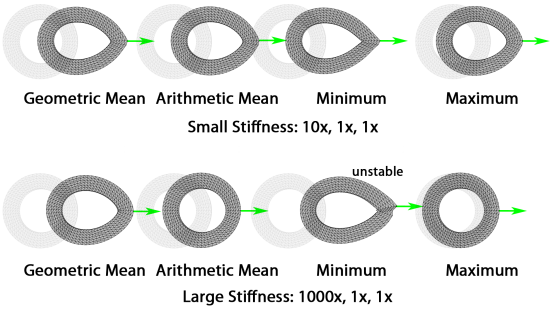

Figure 3: ***Setting the shear modulus for orthotropic materials.*** *The three stiffnesses are radial, longitudinal (in/out the paper), tangential. It can be seen that for small stiffness differences, each method produces acceptable results. For large stiffness differences, we also increased the force strength to generate large deformations. It can be seen that the geometric mean still bends the tube into an ellipse, which is correct given the low tangential stiffness and high radial stiffness. The other three methods cannot reproduce this effect.*

ters, however, easily lead to excessive shear or stiff simulations that lock. It is useful to compute some reasonable μ_{ij} based only on Young's moduli and Poisson's ratios. Therefore, we propose a scheme to set these values automatically. The shear modulus μ of an isotropic material is

$$\mu = \frac{E}{2(1+\nu)}. \tag{21}$$

We extend this equation to set μ_{ij} for orthotropic materials. Since we have found a parameter ν to control all ν_{ij} for orthotropic materials, we can use this parameter in (21). So an equation for a reasonable μ_{ij} of orthotropic materials is

$$\mu_{ij} = \frac{\overline{E}_{ij}}{2(1+\nu)}, \tag{22}$$

for some choice of a scalar $\overline{E}_{ij}$. There are several possible methods to assign $\overline{E}_{ij}$. For example, one can set $\overline{E}_{ij}$ to the maximum, minimum, arithmetic mean or geometric mean of E_i and E_j. Huber [Hub23], followed by other researchers in mechanics [Ber85, CH84], used the geometric mean in predicting shear moduli of reinforced concrete slabs,

$$\mu_{ij} = \frac{\sqrt{E_i E_j}}{2(1+\sqrt{\nu_{ij}\nu_{ji}})}, \tag{23}$$

for $(i,j) = (1,2),(2,3),(3,1)$. Notice that if we use one parameter ν to control all Poisson's ratios, then $\sqrt{\nu_{ij}\nu_{ji}}$ is equal to ν and Huber's formula becomes an example of (22). We also examined other methods (max, min, arithmetic mean), and determined that the geometric mean offers good simulation properties (Figure 3), especially when the three E_i differ by orders of magnitude. First, geometric mean is consistent with the other entries in the elasticity tensor $\mathscr{C}_{ortho}$. Applying (14) and (18) into (6) to (8) yields:

$$A = \frac{1}{(\nu+1)(1-2\nu)} \begin{bmatrix} E_1(1-\nu) & \sqrt{E_1E_2}\nu & \sqrt{E_1E_3}\nu \\ \sqrt{E_1E_2}\nu & E_2(1-\nu) & \sqrt{E_2E_3}\nu \\ \sqrt{E_1E_3}\nu & \sqrt{E_2E_3}\nu & E_3(1-\nu) \end{bmatrix}, \tag{24}$$

$$B = \frac{1}{1+\nu} \begin{bmatrix} \frac{\overline{E}_{12}}{2} & 0 & 0 \\ 0 & \frac{\overline{E}_{23}}{2} & 0 \\ 0 & 0 & \frac{\overline{E}_{31}}{2} \end{bmatrix}. \tag{25}$$

In the upper-left 3×3 block A of $\mathscr{C}_{ortho}$, non-diagonal entries contain a factor $\sqrt{E_iE_j}$. Using geometric mean to compute shear moduli is similar in spirit to this expression. Second, geometric mean considers the magnitude of the Young's moduli in the two directions more evenly than arithmetic mean, especially when the values differ by orders of magnitude. For an orthotropic material where a principal direction with a Young's modulus E_1 is several orders of magnitude stiffer than the other two directions, arithmetic mean would make $\overline{E}_{12}$ and $\overline{E}_{31}$ close to $\frac{E_1}{2}$, and therefore any difference between E_2 and E_3 is ignored for μ_{12} and μ_{31}. Using the geometric mean, however, produces a visible difference between μ_{12} and μ_{31} when E_2 and E_3 themselves differ substantially. In a transversely isotropic material, the shear modulus of the isotropic plane can be derived from E_p and ν_p like with isotropic materials, leaving μ_{zp} as the only free shear parameter. We can assign μ_{zp} as in Equation 22.

5. Results

We demonstrate orthotropic properties using a tube model (Figure 6). We simulate an orthotropic plant (Figures 4), muscle (Figure 5), as well as a flexible dinosaur (Figure 7).

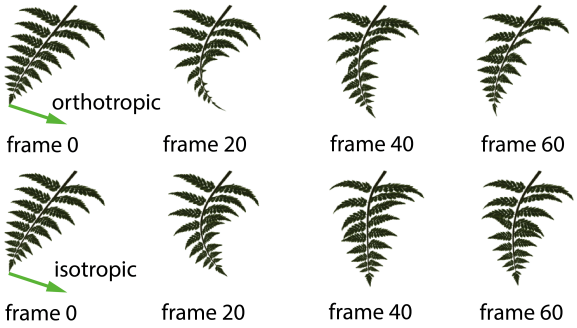

Figure 4: ***Orthotropic vs isotropic plant.*** *This orthotropic fern (top row) has stiffnesses that are 2x, 1x, and 0.01x higher than the isotropic fern (bottom row) in the longitudinal, transverse left-right and transverse up-down directions. We modeled the principal axes to vary along the curved stem, so that they are always orthogonal to the stem. An interesting phenomenon can be observed at frames 20 and 40, similar to buckling: because the left-right direction is much stiffer than the up-down direction, the orthotropic fern's stem rotates (twists), causing most of the deformation to occur in the easiest material direction (up-down), which has now become aligned with the main deformation direction (left-right).*

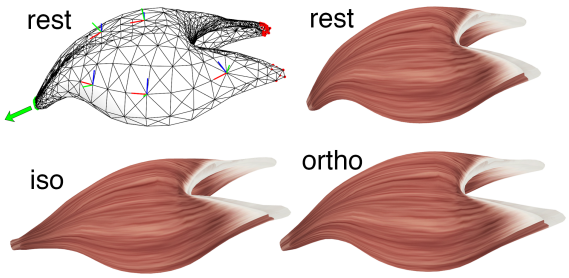

Figure 5: ***Stretched orthotropic muscle.*** *Red vertices are fixed, green vertices are constrained to a fixed displacement. Orthotropic stiffnesses in the up-down (green), transverse (blue) and longitudinal (red) directions are 1000x, 30x and 1x higher than the isotropic stiffness, respectively. The orthotropic muscle preserves the original cross-section more, shrinks less near the attachment points and assumes a more organic shape. Top-left shows the simulation mesh and the spatially varying orthogonal directions.*

	vertices	tets	time	PSC	IFC
dinosaur	344	1,031	0.0060 sec	3	4
muscle	5,014	21,062	0.41 sec	8	12
tube	25,620	129,600	1.2 sec	12	12
fern	298,929	928,088	5.0 sec	12	8

Table 1: *Timestep computation times and the number of employed cores (PSC=Pardiso solver, IFC=internal forces).*

Very small modifications are needed to the isotropic code. Runtime simulation times are unaffected, as we only need to change the computation of the elasticity tensor. This only affects the stiffness matrix computation, which is only done once at startup in a corotational linear FEM simulation. There is only a minor change in the stiffness matrix computation times. For example, the times to construct the isotropic and orthotropic global stiffness matrices were 1993 msec and 2038 msec, respectively (tube example).

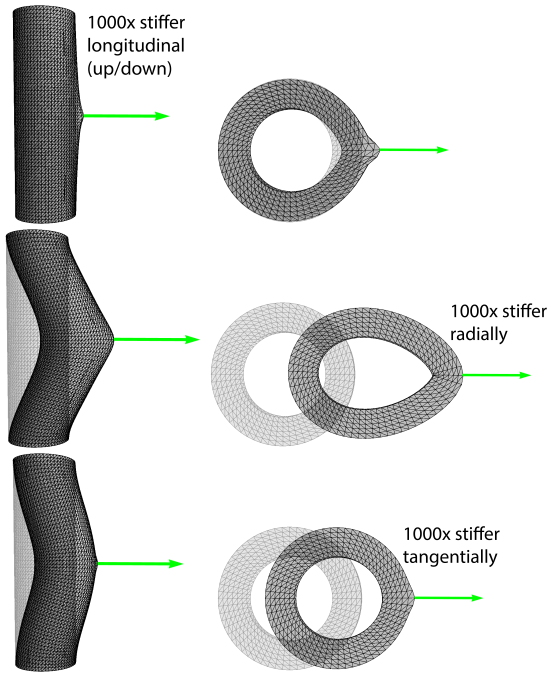

Figure 6: *Static poses for an orthotropic tube, (129,600 tets, 25,620 vertices), under a fixed force load. The right column gives the tube cross-section at the central height where the tube is being pulled. The local orthotropic axes vary across the object: for each element, they point along the longitudinal (up-down), radial and tangential directions. The rows have* $1000\times$ *higher Young's modulus in the longitudinal, radial and tangential tube direction, respectively. In the first row, high Young's modulus in the longitudinal direction prevents the tube from stretching up/down and therefore makes it harder for it to deform sideways. Note the local deformation in the horizontal direction. In the second row, the high radial Young's modulus preserves the thickness of the tube wall, as the tube cannot stretch radially. In the third row, high tangential Young's modulus makes it difficult to stretch the tube along its perimeter, i.e., preserves the perimeter length of the tube; note the radial local deformation.*

6. Conclusion

We have augmented standard corotational linear FEM deformable simulations to support orthotropic materials. We presented a complete modeling pipeline to simulate such materials, which requires minimal changes to existing simulators. We parameterized Poisson's ratios with a single pa-

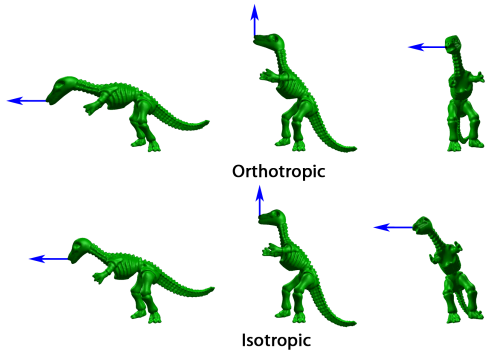

Figure 7: ***Orthotropic vs isotropic dinosaur.*** *The directions in the first, second and third column are* $0.01\times$, $1\times$ *and* $100\times$ *stiffer than the isotropic case.*

rameter and therefore there are orthotropic materials that are not included in our one-dimensional family. For example, with isotropic stiffness ($E_1 = E_2 = E_3$), our one-dimensional family consists of isotropic materials, which excludes orthotropic materials with isotropic stiffness but distinct Poisson's ratios in the three orthogonal directions. Our simulator is also limited to *linear* strain-stress relationships. In the future, we would like to augment it to support general *anisotropic nonlinear* materials. Anisotropic materials would make it possible, for example, to model materials that shear sideways when subjected to a normal load. We would also like to combine our method with inversion-preventing simulations [TSIF05], and investigate orthotropic damping. Implementation of our work is available in Vega FEM 2.1, http://www.jernejbarbic.com/vega.

Acknowledgments: This research was sponsored in part by the National Science Foundation (CAREER-53-4509-6600), USC Annenberg Graduate Fellowship to Yijing Li, and a donation of two workstations by the Intel Corporation.

References

[AMC*09] ALLARD J., MARCHAL M., COTIN S., ET AL.: Fiber-based fracture model for simulating soft tissue tearing. In *Medicine Meets Virtual Reality* (2009), vol. 17, pp. 13–18. 1

[BB98] BONET J., BURTON A.: A simple orthotropic, transversely isotropic hyperelastic constitutive equation for large strain computations. *Computer methods in applied mechanics and engineering 162*, 1 (1998), 151–164. 1

[Ber85] BERT C. W.: Discussion: "Theory of Orthotropic and Composite Cylindrical Shells, Accurate and Simple Fourth-Order Governing Equations". *Journal of Applied Mechanics 52* (1985), 982. 4

[Bow11] BOWER A. F.: *Applied mechanics of solids*. CRC press, 2011. 1

[CH84] CHENG S., HE F.: Theory of orthotropic and composite cylindrical shells, accurate and simple fourth-order governing equations. *J. Appl. Mech. 51* (1984), 736–744. 4

[CTA*08] COMAS O., TAYLOR Z. A., ALLARD J., OURSELIN S., COTIN S., PASSENGER J.: Efficient nonlinear FEM for soft tissue modelling and its GPU implementation within the open source framework SOFA. In *Biomedical Simulation*. Springer, 2008, pp. 28–39. 2

[HJ85] HORN R. A., JOHNSON C. R.: *Matrix Analysis*. Cambridge University Press, 1985. 3

[Hub23] HUBER M.: The theory of crosswise reinforced ferroconcrete slabs and its application to various important constructional problems involving rectangular slabs. *Der Bauingenieur 4*, 12 (1923), 354–360. 4

[ITF04] IRVING G., TERAN J., FEDKIW R.: Invertible Finite Elements for Robust Simulation of Large Deformation. In *Proc. of the Symp. on Comp. Animation* (2004), pp. 131–140. 2

[Lem68] LEMPRIERE B.: Poisson's ratio in orthotropic materials. *AIAA Journal 6*, 11 (1968), 2226–2227. 3

[MG04] MÜLLER M., GROSS M.: Interactive Virtual Materials. In *Proc. of Graphics Interface 2004* (2004), pp. 239–246. 2

[PDA01] PICINBONO G., DELINGETTE H., AYACHE N.: Nonlinear and anisotropic elastic soft tissue models for medical simulation. In *IEEE Int. Conf. on Robotics and Automation* (2001). 1

[PDA03] PICINBONO G., DELINGETTE H., AYACHE N.: Nonlinear anisotropic elasticity for real-time surgery simulation. *Graphical Models*, 5 (2003), 305–321. 1

[PLDA00] PICINBONO G., LOMBARDO J.-C., DELINGETTE H., AYACHE N.: Anisotropic elasticity and force extrapolation to improve realism of surgery simulation. In *IEEE Int. Conf. on Robotics and Automation* (2000), vol. 1, pp. 596–602. 1

[SCD*01] SERMESANT M., COUDIÈRE Y., DELINGETTE H., AYACHE N., DÉSIDÉRI J.-A.: An electro-mechanical model of the heart for cardiac image analysis. In *Medical Image Computing and Computer-Assisted Intervention–MICCAI* (2001), Springer, pp. 224–231. 1

[SDA06] SERMESANT M., DELINGETTE H., AYACHE N.: An electromechanical model of the heart for image analysis and simulation. *IEEE Trans. on Medical Imaging 25*, 5 (2006), 612–625. 1

[Sha90] SHABANA A. A.: *Theory of Vibration, Volume II: Discrete and Continuous Systems*. Springer–Verlag, New York, NY, 1990. 2

[Sif07] SIFAKIS E. D.: *Algorithmic aspects of the simulation and control of computer generated human anatomy models*. PhD thesis, Stanford University, 2007. 2

[SNF05] SIFAKIS E., NEVEROV I., FEDKIW R.: Automatic determination of facial muscle activations from sparse motion capture marker data. *ACM Trans. on Graphics (SIGGRAPH 2005) 24*, 3 (2005), 417–425. 2

[TMD*13] TALBOT H., MARCHESSEAU S., DURIEZ C., SERMESANT M., COTIN S., DELINGETTE H.: Towards an interactive electromechanical model of the heart. *Interface focus 3*, 2 (2013). 1

[TSB*05] TERAN J., SIFAKIS E., BLEMKER S. S., NG-THOW-HING V., LAU C., FEDKIW R.: Creating and simulating skeletal muscle from the visible human data set. *IEEE Trans. on Visualization and Computer Graphics 11*, 3 (2005), 317–328. 2

[TSIF05] TERAN J., SIFAKIS E., IRVING G., FEDKIW R.: Robust Quasistatic Finite Elements and Flesh Simulation. In *Proc. of the Symp. on Comp. Animation* (2005), pp. 181–190. 6

[TTAH07] TEN THIJE R., AKKERMAN R., HUETINK J.: Large deformation simulation of anisotropic material using an updated lagrangian finite element method. *Computer methods in applied mechanics and engineering 196*, 33 (2007), 3141–3150. 1

[VBCW81] VAN BUSKIRK W., COWIN S., WARD R. N.: Ultrasonic measurement of orthotropic elastic constants of bovine femoral bone. *J. of Biomechanical Engineering 103*, 2 (1981), 67–72. 2